Hindawi
Advances in Materials Science and Engineering
Volume 2022, Article ID 9321146, 14 pages
https://doi.org/10.1155/2022/9321146

Research Article

Evaluation of the Contribution Rates of Different Phases on Pavement Performance of Cement-Casting Asphalt Mixture

Minghui Gong,[1,2] **Zijia Xiong**,[1,2] **Lei Jiang**,[1,2] **Cheng Deng**,[1,2] **Sheng Li**,[3] **and Jinxiang Hong**[1,2]

[1]*Jiangsu Sobute New Materials Co. Ltd, 118# Liquan Road, Nanjing, Jiangsu, China*
[2]*State Key Laboratory of High Performance Civil Engineering Materials, 118# Liquan Road, Nanjing, Jiangsu, China*
[3]*Changsha University of Science & Technology, 960#, 2nd Section, Wanjiali Road, Changsha, Hunan, China*

Correspondence should be addressed to Minghui Gong; gongminghui@cnjsjk.cn

Received 20 July 2022; Revised 5 August 2022; Accepted 6 August 2022; Published 6 September 2022

Academic Editor: Shengwen Tang

Cement-casting asphalt mixture (CCAM) exhibits excellent antirutting properties and has been widely used to address the severe rutting distress across the world. However, CCAM's failure mechanism has not been comprehensively understood. To this end, the contribution rates of porous asphalt mixture (PAM), cementitious network, and asphalt-cement interface phases to CCAM's pavement performance are evaluated. A novel method was developed to fabricate the cementitious network with the aid of plastic balls. Abrasion loss, strength, peak force, and fracture energy of PAM, cement samples, and CCAM samples are obtained through different tests. Analysis results show that the contribution rate of cementitious network to Cantabro loss is around 60% and that of the interface phase is around 30%. Interface phase and PAM phase approximately contribute 90% to the overall strength and fracture energy of CCAM. With the increase of polymer contents in asphalt binder, the contribution rate of PAM phase increases and the contribution rate of interface decreases. Contribution rates results together with samples' fracture surface observation verify that the interaction between asphalt skeleton and cement network plays a vital role during CCAM's failure process. Attention should be given to the physical-chemical interactions between asphalt and cement in the future study.

1. Introduction

Cement-casting asphalt mixture has drawn great attention during the past several years in both research and application fields in China [1–5]. It has been widely utilized to address the severe rutting distress of asphalt pavement in heavy-duty sections, such as intersections, BRT lanes, and bus stops [6]. This composite material is fabricated by pouring cementitious slurry into the asphalt mixture skeleton, which takes good advantage of both asphalt mixture and cement concrete [7–16]. Generally, cement-casting asphalt mixture exhibits much better antirutting performance than asphalt mixture, while no joints-cutting is needed. However, field applications have shown that cement-casting asphalt pavement exhibits relatively poorer antirutting cracking properties when compared with traditional asphalt mixture, which limits its further application [17]. Since then, a great number of researchers have been conducting research focusing on the failure mechanism of CCAM.

Hou evaluated the mechanical properties and durability characteristics of CCAM [9]. It was found that the brittleness of hardened cement paste would decrease the low-temperature cracking resistance of CCAM. The properties of CCAM are determined by the internal friction of asphalt mixture skeleton, the network structure of hardened cement paste, and the adhesion between porous asphalt mixture and hardened cement paste. Ding evaluated the influence of volume parameter of asphalt mixture skeleton on the performance of CCAM [18]. As for the asphalt mixture skeleton with the same air voids but different pore structures, it is shown that the performance of CCAM with homogenous gradation is prior to that with consecutive gradation. Ding further investigated the mechanical behavior and failure

mechanism of recycled CCAM with splitting tests [19]. The results revealed that the cracks initially appeared in the recovered binder and the hardened cement paste at the pore connected position. Modified asphalt binder would reduce the residual strain under cyclic loading and therefore delay the development of cracks. Cai evaluated the mechanical features of CCAM with different grouting materials and porous asphalt mixtures with different air voids [20]. The contribution rate and contribution efficiency of each part in the two-phase CCAM are calculated. Specifically, the contribution efficiency refers to the influence of each phase material per volume on the strength of the composite grouting material. According to Cai's research, it was found that the uniaxial compressive strength of CCAM is close to that of grout material, while CCAM's compressive modulus is slightly larger than that of control asphalt mixture. Although CCAM has much better antirutting performance than asphalt mixture, and the contribution rate and contribution efficiency of matrix asphalt mixture to CCAM are larger than those of grouting materials from the perspective of strength [21]. Considering that CCAM consists of open graded asphalt skeleton and the cement skeleton formed through the connected pores in porous asphalt, Cai employed micromechanics to distinguish the different reinforcing mechanism including cement filling skeleton interlock and physiochemical stiffening. Results illustrated that the interlock effect plays a vital role in the stiffness of SFP at low frequencies and porous asphalt mixtures contribute most to the stiffness at high frequencies. The interlock effect would become more stable at higher frequencies as the porosity increases. Afterwards, the damage modes of CCAM under axial compression test were analyzed based on acoustic emission (AE) technique to investigate the failure mechanism of CCAM [22]. Based on these results, the damage processes of CCAM are divided into three phases: (1) compression phase, where the composite material is compressed with little AE signal or damage; (2) microcrack development phase, where the microcrack initiates and develops mostly along the interface between different phases in shearing cracking mode; and (3) macrocrack development phase, where nucleation of microcracks and development of tensile cracks take place to form macrocracks.

Based on the literature review above, it was clearly shown that the mechanical properties of CCAM are determined by asphalt mixture skeleton, grouting material, and the asphalt-cement interface. The contribution rate of asphalt mixture skeleton and grouting material has been quantitatively analyzed [20]. However, the contribution rate of the interface has not been taken into consideration. To this end, this paper aims to develop a method to evaluate the contribution rate of three different phases in CCAM. The findings would hopefully provide an insight into the failure mechanism of CCAM.

2. Objectives

The main objective of this paper is to investigate the contribution rate of different phases on the properties of cement-asphalt composite and provide a guidance for the design of CCAM. Porous asphalt mixture (PAM), cement/cement network, and CCAM cylindrical samples were fabricated in the first step. Afterwards, the pavement performances of different samples were obtained through Cantabro loss test, indirect tension (IDT) test, and semi-circular bending (SCB) test. Finally, the contribution rates of different phases were calculated and compared.

The research flowchart is illustrated in Figure 1.

3. Materials and Tests

3.1. Asphalt Binder. Three different asphalt binders were used. Their basic properties are listed in Table 1. The contents of SBS polymer in SBS modified asphalt and high viscosity modified asphalt are 4% and 14%, respectively.

3.2. Aggregates. Basalt aggregate is used for asphalt mixture fabrication. The aggregates with size from 10 to 16 mm are seized by passing the 9.5 mm mesh screen which is shown in Figure 2. The apparent density of aggregate is 2.94 g/cm^3.

3.3. Asphalt Mixture. The seized single-size aggregates were collected and mixed with asphalt binder at the binder-aggregate ratio of 3%. No fine aggregates or fillers were used. The aggregate was heated to 190°C and asphalt binder was heated to 140°C for base asphalt, 155°C for SBS-modified asphalt, and 165°C for high-viscosity-modified asphalt, respectively. Cylinder samples with two geometries (Φ101.6 mm $*$ 63.5 mm and Φ152.4 mm $*$ 100 mm) were prepared by Marshall compactor. The samples with the size of Φ101.6 mm $*$ 63.5 mm are used for Cantabro loss test and IDT test, while the samples with the size of Φ152.4 mm $*$ 100 mm are prepared for SCB test. The air voids of all samples with different binders were measured and listed in Table 2. It can be seen that all samples exhibit similar air voids around 32%, which makes sure that the differences in the pavement performance of CCAM come from PAM and the interactions between cement and different binders. The influences of grouting material type and grouting material content in CCAM which is directly related to the air voids of PAM are not considered in this research.

3.4. Grouting Material. Grouting material is developed by mixing the cement with filler and admixtures. The water/binder ratio is set as 0.36. The grouting slurry is prepared by using a high shear mixer. Properties of grouting slurry are displayed in Table 3.

3.5. Cementitious Sample. Cylinder cementitious samples were prepared by pouring the grouting slurry into the polyvinyl chloride (PVC) tubes with the same size as the Marshall asphalt mixture samples (shown in Figure 3). The bottom surfaces of PVC samples were sealed with tape.

To simulate the actual state of cement in CCAM, plastic balls with the diameter of 1 cm were used to fill in the PVC tubes and work as the skeleton (shown in Figure 4) [23].

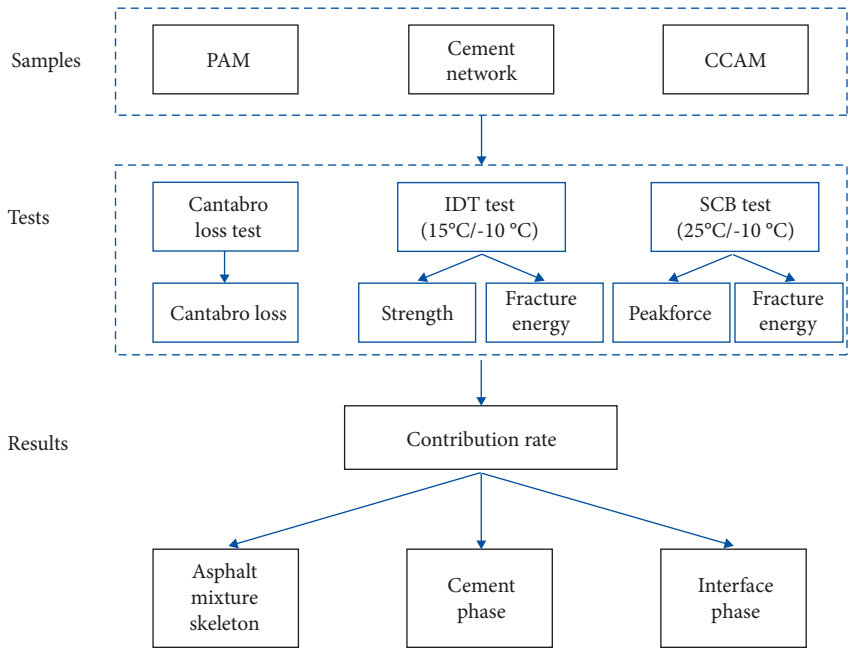

Figure 1: Research flowchart.

Table 1: Basic properties of asphalt binders.

Property	Pen 70 asphalt	SBS-modified asphalt	High-viscosity-modified asphalt
Penetration (25°C, 100 g, 5 s)/0.1 mm	68	53	45
Softening point (Ring & Ball method)/°C	48	68	95
Ductility (5°C, 5 cm/min)/cm	—	25	38
Viscosity (165°C)/Pa.s	0.16	0.923	3.06

Figure 2: Aggregates (left: before being seized; right: after being seized).

Table 2: Air voids of cylinder asphalt mixture samples.

Sample size	Air voids/%		
	Pen 70 asphalt	SBS-modified asphalt	High-viscosity-modified asphalt
Φ101.6 mm * 63.5 mm	32.18	31.60	31.38
Φ152.4 mm * 100 mm	32.18	33.16	31.82

Grouting materials were then poured into the PVA tubes. For PAV tubes with plastic balls, a metal mesh was used to cover the top of the tubes during grouting to prevent the plastic balls from floating out of the tubes. After curing for 7 days, the samples were got out of the tubes. The cementitious samples with and without balls are demonstrated in Figure 5. By counting the number of plastic balls, the volume of plastic ball skeleton can be calculated and the residue volume of

Table 3: Properties of grouting slurry.

Property		Test result
Fluidity/s	0 min	12
	30 min	16
Compressive strength/MPa	3 h	12
	1 d	20

Figure 3: PAV tubes for fabrication of the cementitious sample.

Figure 4: PAV tubes filled with plastic balls.

grouting material can be obtained. The volumetric percentage of the cementitious network was determined as 17.3%.

3.6. CCAM Samples. The PAM samples were firstly sealed with tape. Grouting materials were then poured into the sealed PAM samples. In the end, these samples were cured in the ambient environment with a temperature of 22°C and humidity of 50% for 7 days.

4. Pavement Performance Characterization

Cantabro loss test and indirect tensile test were conducted according to Standard Test Methods of Bitumen and Bituminous Mixtures for Highway Engineering [24]. Semicircular bending test was conducted according to AASHTO Standard Method of Test for Determining the Fracture Potential of Asphalt Mixtures Using Semicircular Bend Geometry (SCB) at Intermediate Temperature [25].

IDT tests were conducted at 15°C and −10°C. The loading rates were set as 50 mm/min and 1 mm/min, respectively. Indirect tension strengths were calculated as follows:

$$ITS = \frac{0.006287P}{h}, \tag{1}$$

where ITS is indirect tension strength, MPa; P is peak force, N; and h is the height of Marshall sample, mm.

For SCB tests, 25°C and −10°C were chosen as the test temperatures. The corresponding loading rates were 50 mm/min and 1 mm/min, respectively. The height, thickness, and diameter of SCB specimen were 50 mm, 50 mm, and 150 mm, respectively. The notch depth and width are set as 15 mm and 1.5 mm, respectively.

Fracture energy (Gf) can be expressed as

$$G_f = \frac{W_f}{ligament\ length \times specimen\ thickness} \times 10^6. \tag{2}$$

G_f is fracture energy, J/m^2; W_f is the work of fracture, J.

Pavement performances of different samples, including Cantabro loss, IDT strength, IDT fracture energy, SCB peak force, and SCB fracture energy, were then compared and analyzed.

5. Contribution Rate Calculation

The contribution rates of different phases are calculated as follows:

$$\begin{aligned} k_A &= \frac{1}{E_A} / \frac{1}{E_C}, \\ k_G &= \frac{1}{E_G} / \frac{1}{E_C}, \\ k_I &= 1 - k_A - k_G, \end{aligned} \tag{3}$$

where k_A, k_G, and k_I are the contribution rates of PAM phase, grouting cementitious network phase, and interface phase, respectively.

E_A, E_G, and E_C represent the pavement performance (e.g., Cantabro loss, strength, peak force, and fracture energy) of PAM phase, grouting cementitious network phase, and CCAM, respectively.

The contribution of interface phase on the overall strength of CCAM comes from the bonding between cement and asphalt as well as the friction between asphalt mixture skeleton and grouting network.

6. Results and Discussion

6.1. Cantabro Loss Test. The Cantabro losses of base asphalt mixture (BAM), SBS-modified asphalt mixture (SAM), and high-viscosity-modified asphalt mixture (HAM) are demonstrated in Figure 6. As single-size aggregates were used, all PAM's Cantabro losses are higher than 80%. The anti-raveling ability of PAM can be enhanced by using high-

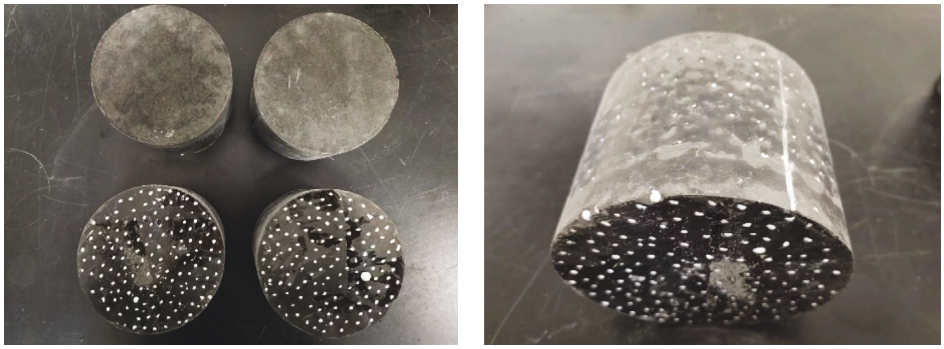

(a) (b)

Figure 5: Cementitious samples with and without balls. (a) Top view. (b) Side view.

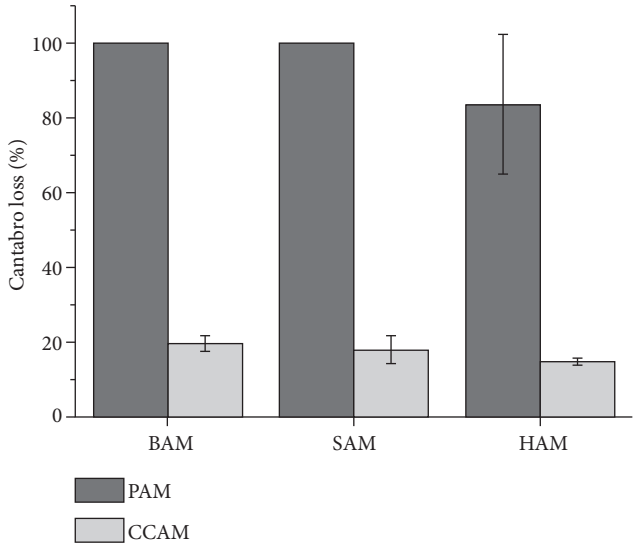

Figure 6: Cantabro losses of mixtures before and after grouting.

viscosity-modified asphalt. It is clearly shown that cement-grouting would significantly decrease the Cantabro loss of PAM. As the viscosities of asphalt binders increase, the Cantabro losses of CCAM go down slightly.

Table 4 illustrates the Cantabro losses of cement samples with and without plastic balls. It is found that cement sample has much better antiraveling ability than PAM but worse antiraveling ability than CCAM. The Cantabro loss of the cement sample with balls is about twice as much as that of the cement sample with no balls. Samples of CCAM and cement samples after test are shown in Figure 7.

6.2. IDT Test. Force-displacement curves of PAM, CCAM, and cement samples are shown in Figure 8. For IDT test at 15°C, it is found that CCAM and cement sample without balls show similar peak forces. Cement sample with balls has the lowest peak force among all samples. Both the cement samples with and without balls display brittleness characteristics as the force drops quickly after peak force. When the test is conducted at −10°C, the peak force of cement sample without balls is close to that of CCAM. However, the displacement at the peak force of cement sample with balls is

Table 4: Cantabro losses of cement samples.

Sample	Cantabro loss/%	Coefficient of variation (CV)/%
Cement sample with no balls	22.3	5.1
Cement sample with balls	47.0	2.2

higher than that of cement sample without balls. This can be attributed to the existence of plastic balls. The balls hardly provide any contribution to the strength of CCAM at 15°C but may become brittle at low temperatures which impacts the failure process of cement sample with balls. Nevertheless, the peak force of cement sample without balls is still much higher than that of the cement sample with balls which proves that the stability of fabricated cementitious network is much lower than that of the integral cementitious sample.

The pictures of the fractured samples are shown in Figure 9. It is shown that the cracks generally develop along with two routines for the cement sample without balls. The samples were fractured into three pieces. For the cement samples with balls, the crack mainly develops along with the plastic ball-cement interface and through the cement matrix. The plastic balls would distract the stress concentration during loading. Figures 10 and 11 demonstrate the IDT strength and fracture energy results of PAM and CCAM samples, respectively. Typically, using polymer-modified asphalt would slightly increase the strength of PAM but lower the strength of CCAM. However, both PAM and CCAM's fracture energies at 15°C would increase as more polymers were used in asphalt. At −10°C, SAM has the highest fracture energy among the three kinds of mixtures. HAM-PAM exhibits higher fracture energy than BAM-PAM, while HAM-CCAM's fracture energy is lower than that of BAM-PAM. This can be attributed to the failure mode of PAM. It has been pointed out in the literature that cohesive failure is the main cause at high temperatures, while adhesive failure is predominant at low temperatures of PAM. Although high viscosity asphalt binder was used, the failure mainly takes place in the asphalt-aggregate interface at low temperature [26, 27]. Thus, the high cohesion energy of high viscosity asphalt binder cannot be fully taken advantage of. IDT strength and fracture energy of cement samples are

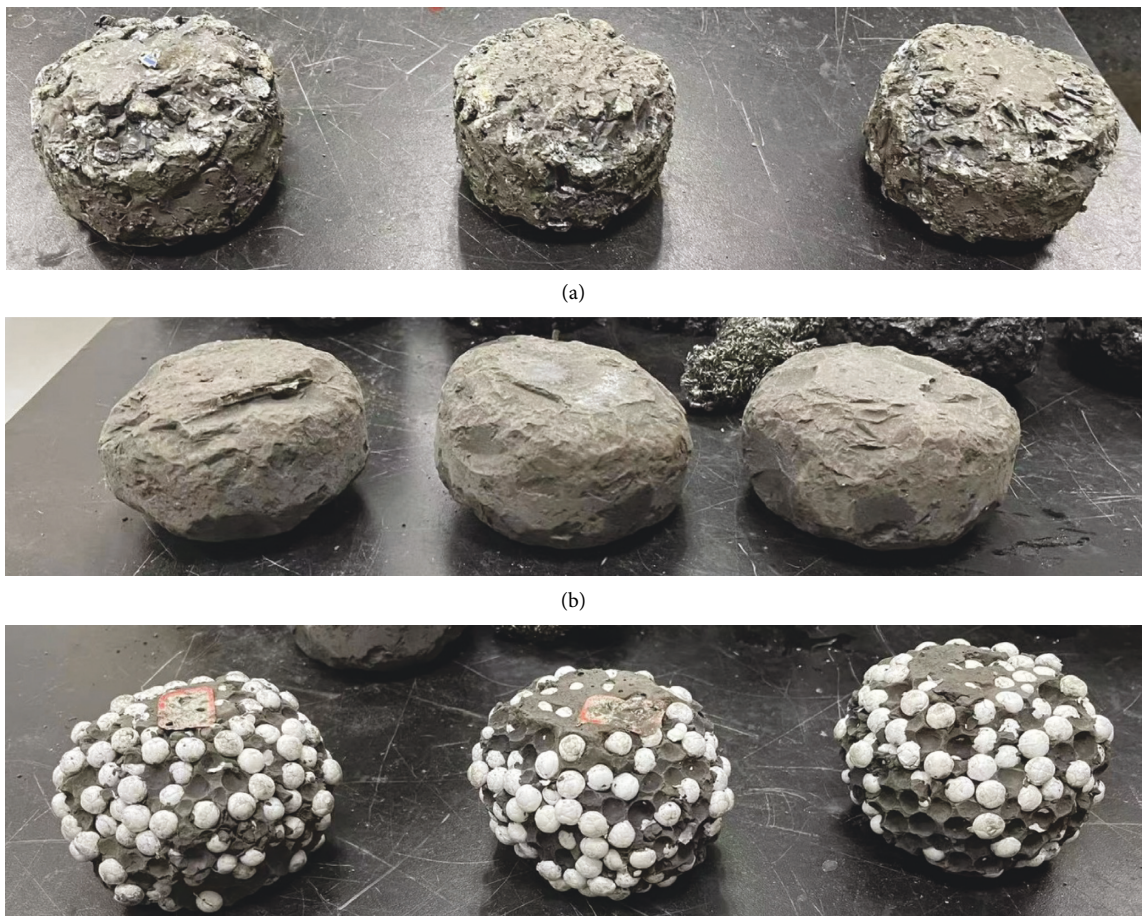

(a)

(b)

(c)

Figure 7: Samples after Cantabro loss testing. (a) CCAM. (b) Cement sample with no balls. (c) Cement sample with balls.

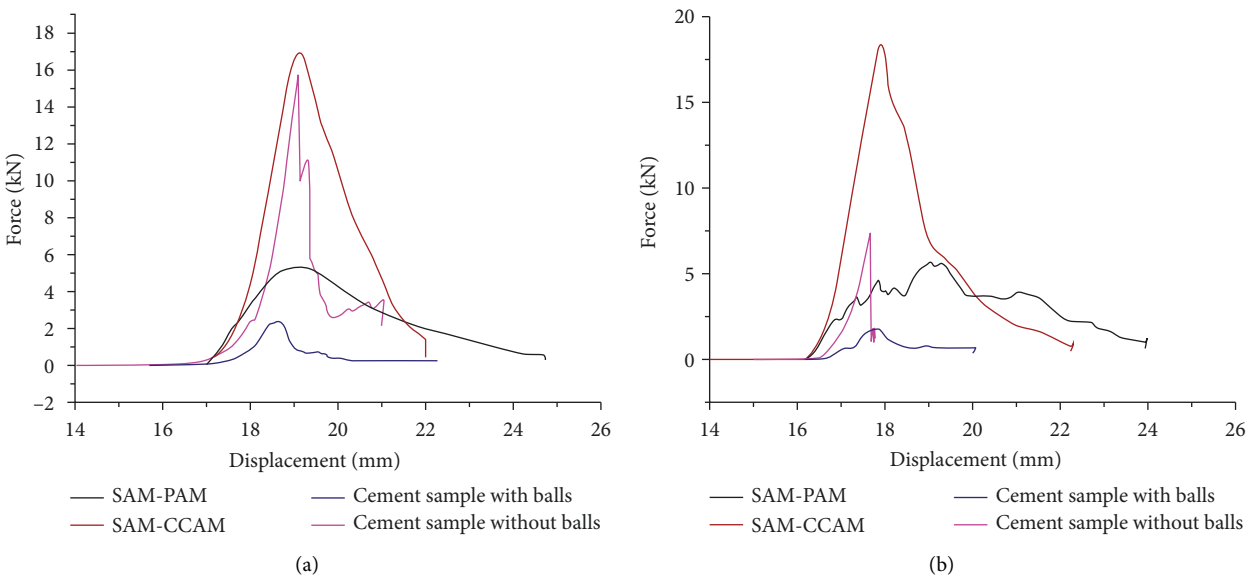

Figure 8: Force-displacement curves of samples from the IDT test. (a) 15°C. (b) −10°C.

(a) (b)

Figure 9: Fractured IDT samples. (a) Top view. (b) Side view.

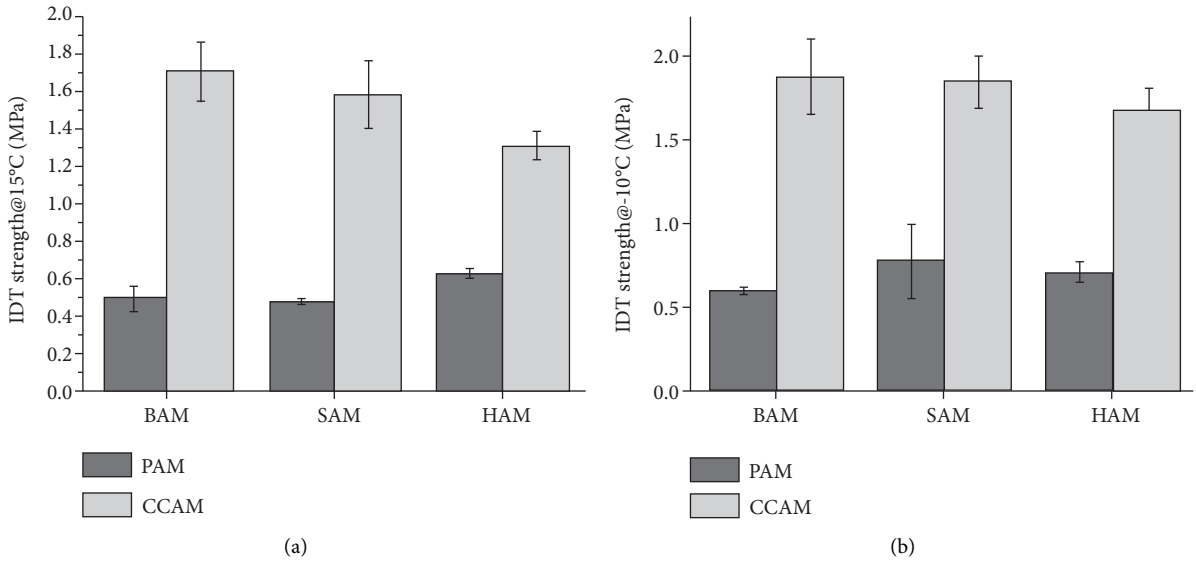

(a) (b)

Figure 10: IDT strengths of PAM and CCAM samples. (a) 15°C. (b) −10°C.

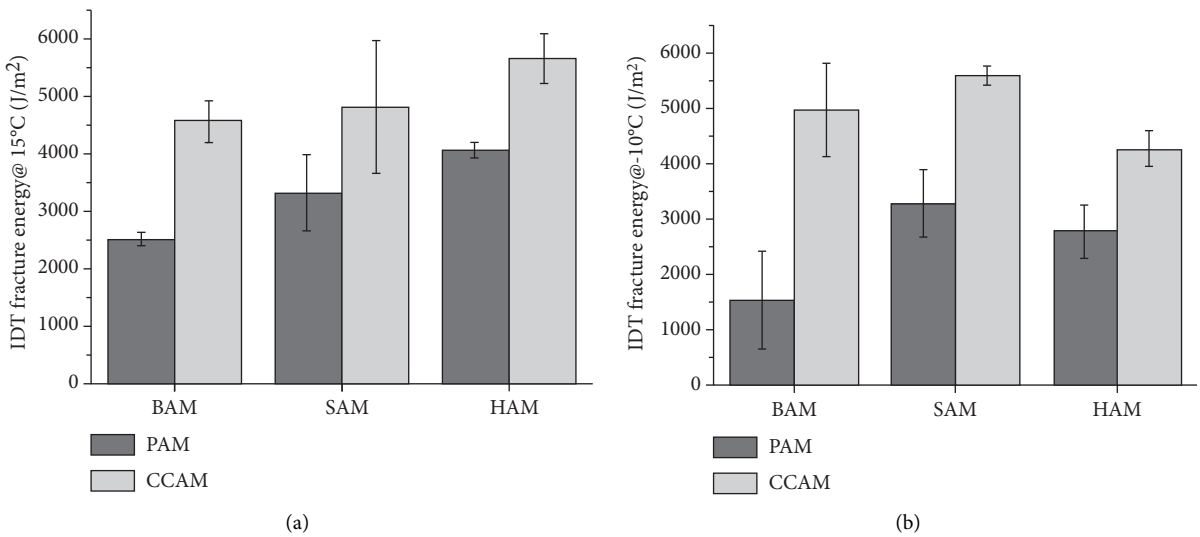

(a) (b)

Figure 11: IDT fracture energy of PAM and CCAM samples. (a) 15°C. (b) −10°C.

illustrated in Table 5. The strength of cement samples without balls is around six times higher than that of cement samples with balls at 15°C and about four times higher than that of cement samples with balls at −10°C. The 15°C fracture energy of cement sample without balls is much higher than that of cement samples with balls. However, the difference between the fracture energies of these two samples at −10°C was not as distinct as at 15°C.

Table 5: IDT strength and fracture energy of cement samples.

Sample	IDT strength @ 15°C/MPa	CV/%	IDT strength @ −10°C/MPa	CV/%
Cement sample with no balls	1.22	34.9	0.85	17.5
Cement sample with balls	0.23	14.2	0.21	22.4
Sample	IDT fracture energy @ 15°C/J/m^2	CV/%	IDT fracture energy @ −10°C/J/m^2	CV/%
Cement sample with no balls	2175.688	26.2	605.5345	23.3
Cement sample with balls	530.6177	5.0	397.3175	10.1

6.3. SCB Test. SCB force-displacement curves of the samples are shown in Figure 12. At 25°C, CCAM sample has much higher strength than other samples. However, CCAM and cement samples without balls exhibit similar peak force values at −10°C. Regardless of the test temperature, the peak force value of the cement sample with balls is the lowest among all the samples. Unlike IDT test results, Figure 12 shows that CCAM behaves more like a cement sample rather than PAM. The differences can be attributed to the loading mode. The sample loses its strength due to tensile failure in IDT test, while the sample fails due to flexural bending in SCB test. The cementitious materials in CCAM make the composite materials more sensitive to flexural failure.

Pictures of failed samples are demonstrated in Figure 13. There are visible cracks in CCAM, cement sample with balls, and cement samples without balls except PAM. It is shown that there are some similarities in the crack development patterns between CCAM and cement sample with balls. The cracks mainly develop across the cement phase and along the cement-aggregate/ball interface. SCB peak forces and fracture energies of PAM and CCAM samples are further displayed in Figures 14 and 15, respectively. It is found that using polymer would slightly increase the peak force of PAM at 25°C. The increase would become relatively distinct at −10°C. BAM-CCAM has the highest peak force among CCAM samples at 25°C. But the differences among the peak forces of BAM-CCAM, SAM-CCAM, and HAM-CCAM at −10°C are not significant. For fracture energy data, there is a clear trend that more polymer in asphalt binder would correspond to higher fracture energies in PAM and CCAM. It is shown that PAMs have higher fracture energies than CCAMs for all three kinds of mixtures at 25°C. This phenomenon shows that cementitious grouting would decrease the anticracking ability of PAM. Contrarily, all CCAMs show higher fracture energies than their PAMs. This verifies that different phases have different mechanical responses to loading at different temperatures. PAM becomes stiffer at low temperature and cementitious network can reinforce its anticracking ability. It is notable that all the PAM's fracture energy data show high variance. This can be explained as that the strength of PAM is formed by point-point stone contact [26, 27]. The crack develops more randomly and scatteringly in PAM which can also be reflected in the PAM force-displacement curve in Figure 12.

Table 6 illustrates the SCB peak force and fracture energy of cement samples at 25°C and −10°C. It is shown in the IDT test that cement samples have similar strengths at 15°C and −10°C. However, The SCB peak force of cement sample at −10°C is about twice higher than that at 25°C. Moreover, the peak force of cement samples without balls is around three to four times higher than that of cement samples with balls. This again indicates that the failure mechanisms of samples in SCB and IDT tests are different. The SCB fracture energies of cement samples are much lower than those of PAM and CCAM. It seems that the cementitious network alone does not have the potential to make PAM as tough as CCAM. The interface phase should also have vital contributions to the anticracking ability of CCAM. However, the contribution rate of cement-asphalt interface has not been evaluated in the literature.

6.4. Contribution Rate Analysis. The contribution rates of PAM phase, cementitious network phase, and interface phase are calculated according to equation (3) to (5) and illustrated in Table7 in sequence. As the cementitious network was fabricated for the first time, the cementitious network phase's contribution rate is acquired by using test data from both cement samples with balls and without balls to see if there are significant differences between them.

As can be seen in Table 7, the contribution rate of cement phase is much higher than that of cementitious network especially for IDT and SCB test results. By using the data from the cement sample without balls, the contribution from cement phase to the overall performance of CCAM is overestimated and the contribution from interface phase is underestimated. For Cantabro loss test result, PAM almost contributed nothing to CCAM's antiraveling ability. The contribution rate of cementitious network is around 60% and that of interface phase is around 30%. The contribution rates of different phases for BAM and SAM are close with each other. Unlike Cantabro loss test result, the interface phase contributes most to the IDT strength at 15°C and −10°C, while cementitious network phase contributes least. As more polymer modifiers are used, the contribution rate of interface phase to IDT strength decreases, while the contribution rates of PAM and cementitious network increase. When referring to SCB test results, similar trends can also be found. Higher viscosity of asphalt binder would lower the contribution rate of interface phase while increasing the other two phases' contribution rates. At −10°C, the contribution rate of cementitious network to SCB peak force is relatively stable. For SAM and HAM samples, PAM phases contribute more to the SCB peak force than the interface phases.

Due to space limitation, the contribution rates calculated using the data of cement sample without balls are not shown further. The contribution rates of the three phases to IDT and SCB fracture energy are demonstrated in Figures 16 and 17. The contribution rates of PAM in SAM and HAM are

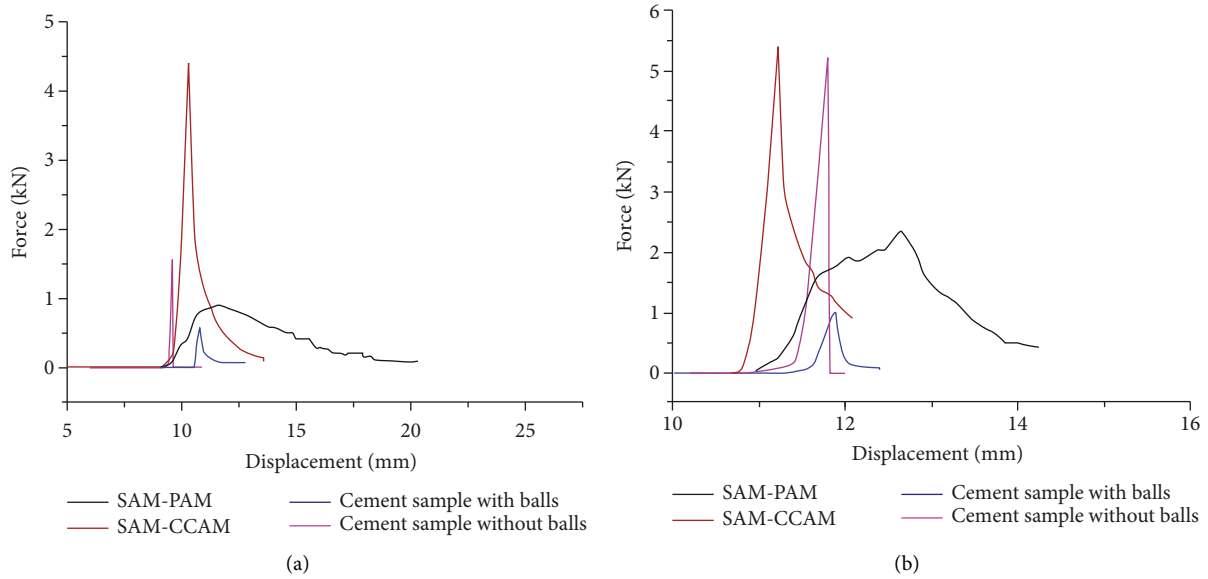

Figure 12: Force-displacement curves of samples from the SCB test. (a) 25°C. (b) −10°C.

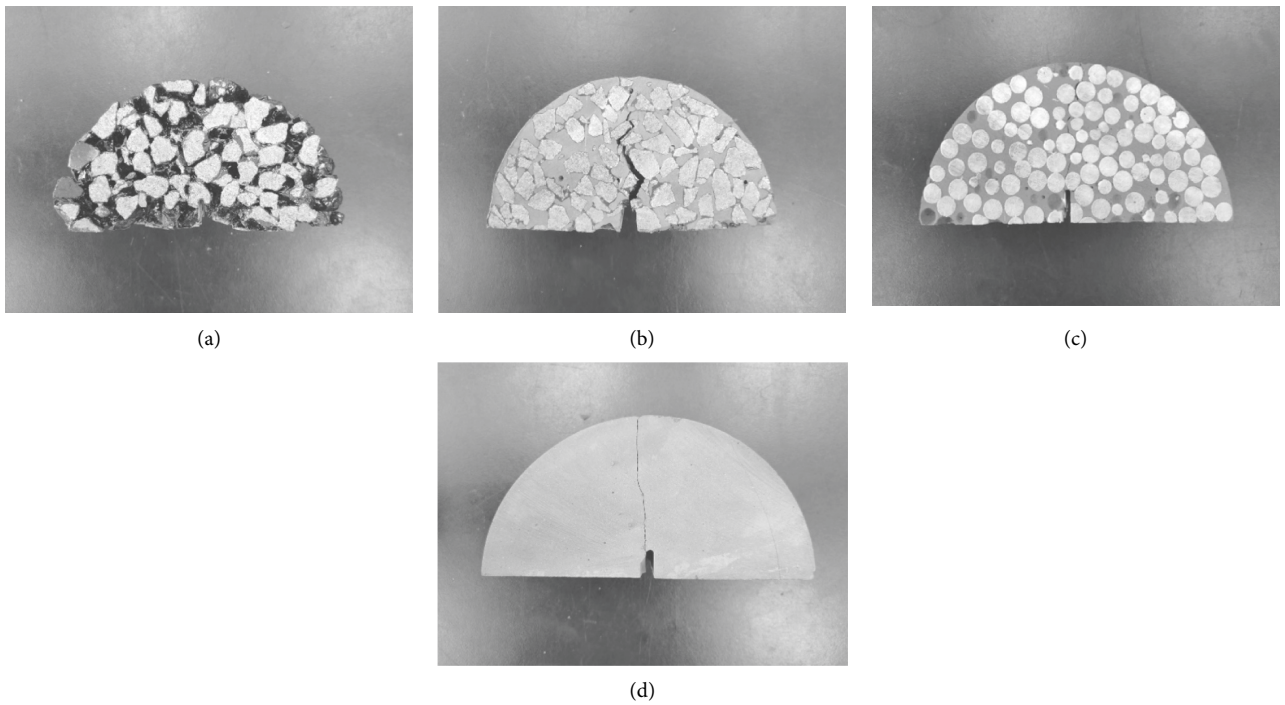

Figure 13: Failed SCB samples. (a) PAM. (b) CCAM. (c) Cement sample with no balls. (d) Cement sample with no balls.

similar. Besides PAM, the interaction between asphalt and cement also plays a vital role in the contribution to the IDT fracture energy especially at lower temperature. The bonding together with friction between asphalt mixture skeleton and grouting network becomes dominated. When looking at Figure 17, it is interesting to find that the contribution rate of the interface phase to SCB fracture energy at 25°C is negative. This phenomenon can be explained as that the interface between PAM and cementitious network may be the weak zone of CCAM. At higher temperatures PAM would become soft and deform more under same loading. However, the existence of cementitious network would limit the deformation of PAM. Due to different modulus of cement and asphalt materials, the discontinuous displacement of cement network and PAM at the interface would induce stress concentration. The temperature would also influence the bonding strength and friction between PAM and cementitious network. All these together contribute to the different contribution rates of interface phase at different temperatures. The grouted cementitious materials can be

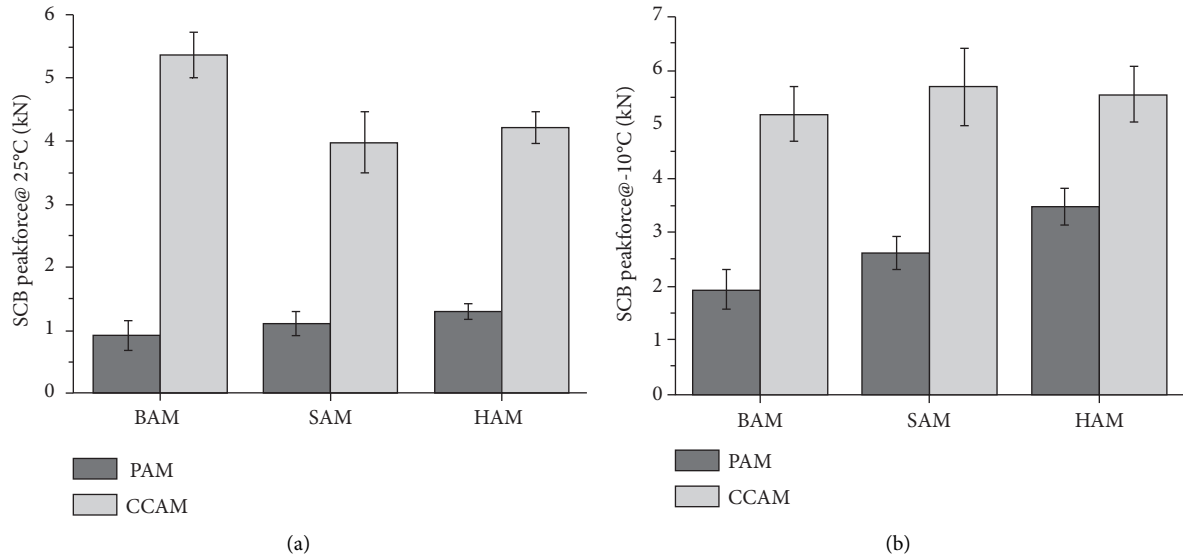

Figure 14: SCB peak forces of PAM and CCAM samples. (a) 25°C. (b) −10°C.

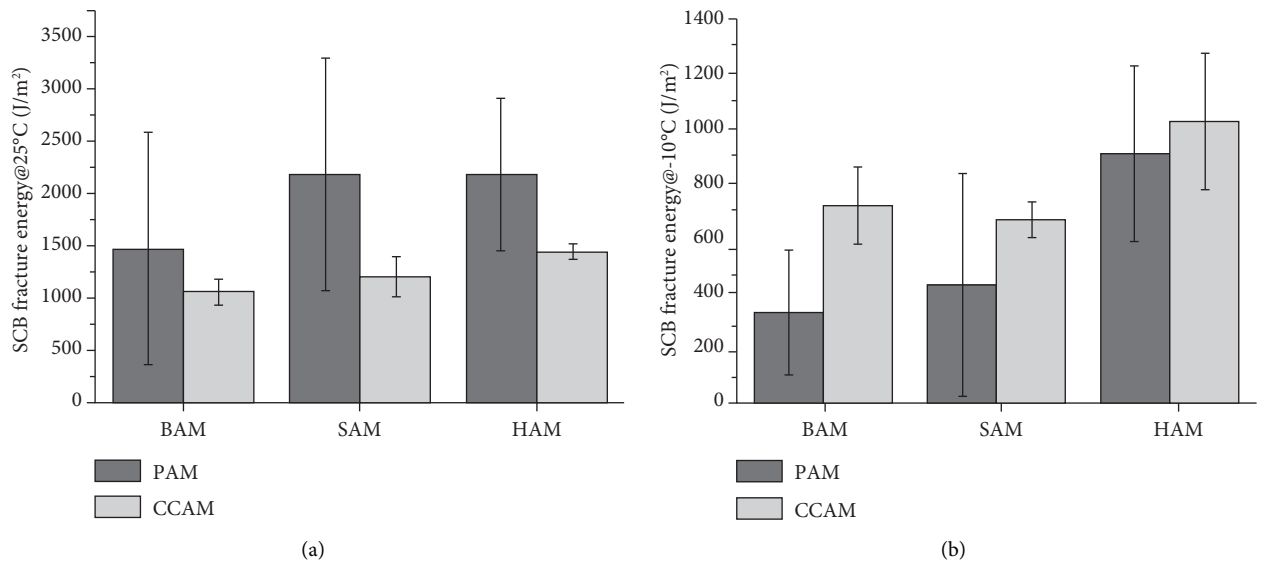

Figure 15: SCB fracture energies of PAM and CCAM samples. (a) 25°C. (b) −10°C.

Table 6: SCB peak force of cement samples.

Sample	SCB peak force @ 25°C/kN	CV/%	SCB peak force @ −10°C/kN	CV/%
Cement sample with no balls	1.72	9.2	3.61	29.7
Cement sample with balls	0.52	13.0	0.97	9.3
Sample	SCB fracture energy @ 25°C/J/m^2	CV/%	SCB peak force @ −10°C/J/m^2	CV/%
Cement sample with no balls	68.1	29.9	240.9	25.7
Cement sample with balls	92.9	25.7	69.08	29.3

regarded as a reinforcing phase from the perspective of SCB fracture energy at 25°C. As discussed in Figure 13, the crack in PAM develops more randomly and scatteringly across the asphalt binder phase. Moreover, there exists a compression force from the loading strip in the top part of PAM during loading at 25°C. Since there are large-size air voids between aggregates in PAM, the space between aggregates would be squeezed. As reflected in the force-displacement curve, it will show that the PAM deforms more under loading. This crack development pattern and compression induced deformation

Table 7: Contribution rates of different phases to the mechanical properties of CCAM.

Mixture type	Contribution rate to Cantabro loss/(%)		
	Interface (without balls)	PAM (without balls)	Cement (without balls)
BAM	3.27	0	96.73
SAM	5.36	0	94.64
HAM	1.3	17.17	81.52
	Interface (with balls)	PAM (with balls)	Cementitious network (with balls)
BAM	34.02	0	65.98
SAM	35.44	0	64.55
HAM	27.21	17.17	55.61
Mixture type	Contribution rate to IDT strength @ 15°C/(%)		
	Interface (without balls)	PAM (without balls)	Cement (without balls)
BAM	−0.59	28.82	71.76
SAM	−6.96	29.75	77.22
HAM	−38.35	46.62	91.73
	Interface (with balls)	PAM (with balls)	Cementitious network (with balls)
BAM	58.23	28.82	12.94
SAM	56.33	29.75	13.92
HAM	36.84	46.62	16.54
Mixture type	Contribution rate to IDT strength @ −10°C/(%)		
	Interface (without balls)	PAM (without balls)	Cement (without balls)
BAM	22.87	31.91	45.21
SAM	12.36	41.93	45.69
HAM	6.54	42.85	50.59
	Interface (with balls)	PAM (with balls)	Cementitious network (with balls)
BAM	58.51	31.91	9.57
SAM	48.39	41.93	9.68
HAM	46.43	42.85	10.71
Mixture type	Contribution rate to SCB peak force @ 25°C/(%)		
	Interface (without balls)	PAM (without balls)	Cement (without balls)
BAM	50.49	17.45	32.06
SAM	28.96	27.69	43.35
HAM	29.49	29.62	40.89
	Interface (with balls)	PAM (with balls)	Cementitious network (with balls)
BAM	72.93	17.45	9.62
SAM	59.29	27.69	13.01
HAM	58.11	29.62	12.27
Mixture type	Contribution rate to SCB peak force @ −10°C/(%)		
	Interface (without balls)	PAM (without balls)	Cement (without balls)
BAM	−9.89	37.31	72.58
SAM	−12.3	46	66.3
HAM	−28.75	59.81	68.93
	Interface (with balls)	PAM (with balls)	Cementitious network (with balls)
BAM	44.08	37.31	18.61
SAM	37.0	46	16.99
HAM	22.52	59.81	17.67

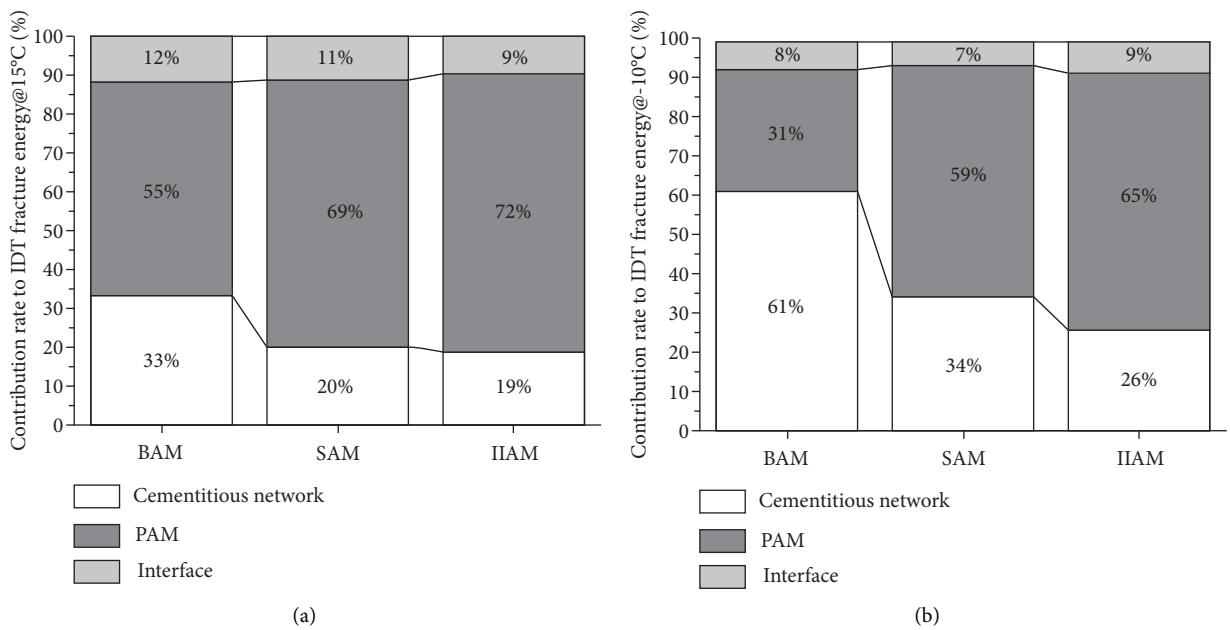

Figure 16: Contribution rates to IDT fracture energy. (a) 15°C. (b) −10°C.

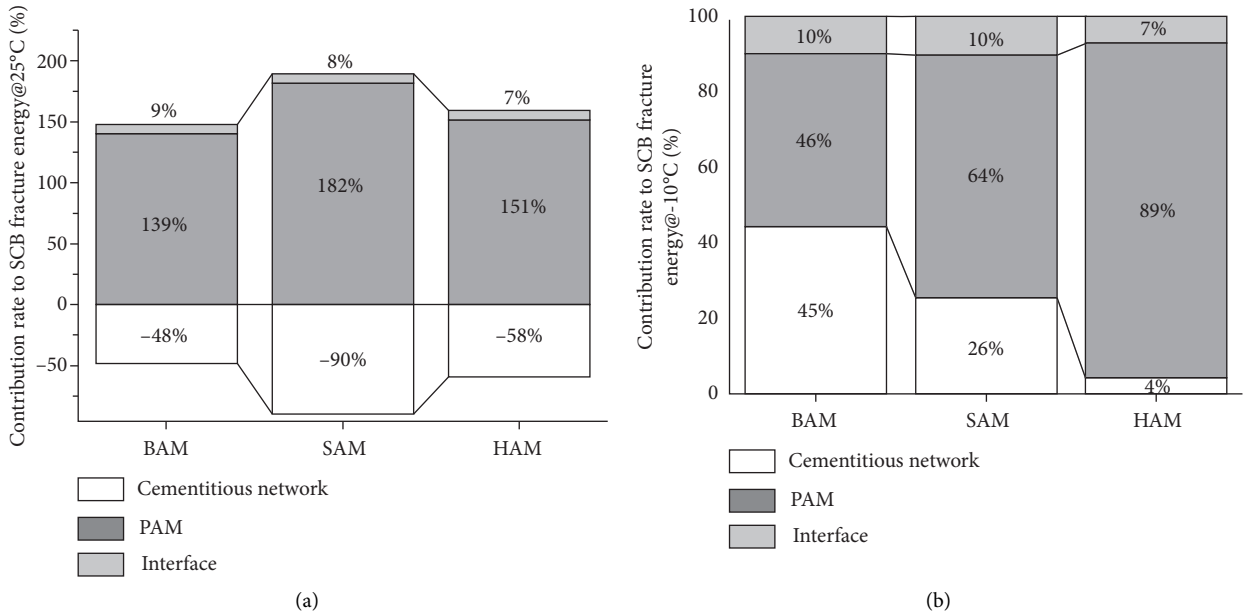

Figure 17: Contribution rates to SCB fracture energy. (a) 25°C. (b) −10°C.

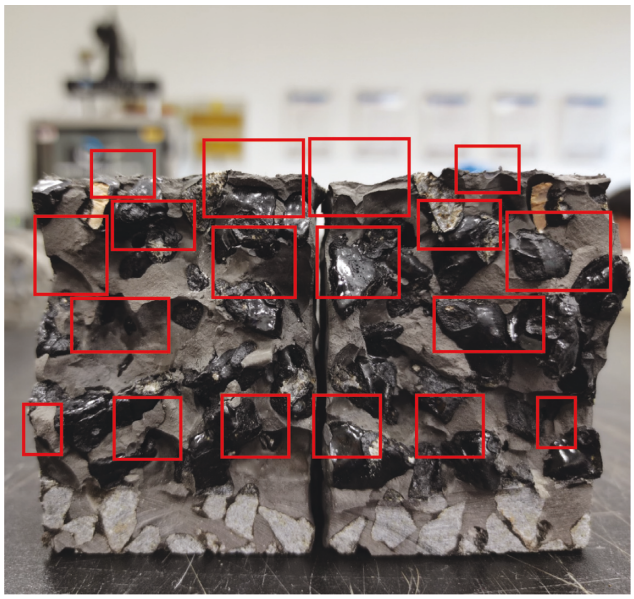

Figure 18: Fracture surface of CCAM.

would together make the fracture energy higher. However, as pointed out by Cai, the compression in CCAM will be transformed into tension and interfacial shearing force [21]. As can be seen in Figure 18, the fracture surface of CCAM mainly contains cement fracture, asphalt binder cohesive failure, and asphalt-cement adhesive failure (marked as red). Both cement fracture and asphalt-cement adhesive failure would contribute much lower fracture energy than asphalt binder cohesive failure. At −10°C, all the contribution rates for SCB test results are positive. Similar to IDT results, PAM contributes most to the fracture energy at −10°C and the contribution rate keeps increasing as more polymers are used in the mixture.

7. Conclusions

The main objective of this paper is to evaluate the contribution rates of asphalt skeleton, cement, and interface phases on the pavement performance of CCAM. The cementitious network is simulated by using plastic balls with a diameter of 1 cm as single-seized aggregates. The Cantabro loss test, IDT test, and SCB test were employed to characterize the performance of PAM, CCAM, and cement samples with and without balls. The main conclusions are drawn as follows:

(1) Cement sample with balls generally has higher Cantabro loss, lower IDT strength/fracture energy, and lower SCB peak force/fracture energy than cement sample without balls.

(2) By using the data from cement sample without balls, it is found that the contribution from cement phase to the overall performance of CCAM is overestimated and the contribution from interface phase is underestimated.

(3) The contribution rate of cementitious network to Cantabro loss is around 60% and that of interface phase is around 30%. Interface phase and PAM phase approximately contribute 90% to the overall strength and fracture energy of CCAM. With the polymer contents in the asphalt binder increasing, the contribution rate of PAM phase increases and the contribution rate of interface decreases.

(4) It is inferred that the formation of an interface between PAM and cementitious network would change the developing routines of cracks in PAM. The crack in PAM is formed due to asphalt binder cohesion failure between aggregates under tensile force, while the crack in CCAM consists of asphalt binder

cohesion failure, cement failure, and asphalt-cement interface adhesive failure. The result in this paper verifies that the asphalt-cement interface adhesive failure is nonnegligible.

Data Availability

Data are available upon request from the authors.

Additional Points

Limitations. (1) As only one type of grouting material is used in this paper, the contribution rate of cementitious network is relatively stable. Combinations of different types of asphalt binder and grouting materials can be used in future research to comprehensively evaluate the contribution rates of different phases in CCAM. (2) Although it is assumed that light-weight plastic balls would have no interactions with cement and they can be regarded as air bubbles in the samples, some clues from the force-displacement curve in −10°C IDT test were found that the elasticity of plastic balls may slightly impact the test results. (3) The aggregate is not perfectly round and the diameter is not exactly 1 cm. Therefore, the air void of the fabricated PAM is 32%, while the volume within the plastic ball skeleton is 17%. There is still a gap between PAM and the fabricated plastic ball skeleton.

Conflicts of Interest

The authors declare that they have no conflicts of interest.

Acknowledgments

The authors acknowledge the National Key Research and Development Program of China (no. 2021YFB2601000), Natural Science Foundation of Jiangsu (no. BK20210058), and Science and Technology Progress and Innovation Plan Project of Hunan Provincial Department of Transportation (no. 202111).

References

[1] Z. Xiong, M. Gong, S. Wang, C. Deng, and J. Hong, "Evaluation of the failure behavior of cement grouted asphalt mixture with different grouting materials and asphalt binders," *Int. J. Pavement Res. Technol*, vol. 15, no. 4, pp. 957–969, 2021.

[2] M. Gong, Z. Xiong, C. Deng, G. Peng, L. Jiang, and J. Hong, "Investigation on the impacts of gradation type and compaction level on the pavement performance of semi-flexible pavement mixture," *Construction and Building Materials*, vol. 324, Article ID 126562, 2022.

[3] W. Zhao and Q. Yang, "Study on the applicability of asphalt concrete skeleton in the semi-flexible pavement," *Construction and Building Materials*, vol. 327, Article ID 126923, 2022.

[4] S. Wang, H. Zhou, X. Chen, M. Gong, J. Hong, and X. Shi, "Fatigue resistance and cracking mechanism of semi-flexible pavement mixture," *Materials*, vol. 14, no. 18, p. 5277, 2021.

[5] S. Ling, Y. Sun, D. Sun, and D. Jelagin, "Pore characteristics and permeability simulation of porous asphalt mixture in pouring semi-flexible pavement," *Construction and Building Materials*, vol. 330, Article ID 127253, 2022.

[6] Y. Du, J. Chen, Z. Han, and W. Liu, "A review on solutions for improving rutting resistance of asphalt pavement and test methods," *Construction and Building Materials*, vol. 168, pp. 893–905, 2018.

[7] I. L. Al-Qadi, H. Gouru, and R. E. Weyers, "Asphalt portland cement concrete composite: laboratory evaluation," *Journal of Transportation Engineering*, vol. 120, no. 1, pp. 94–108, 1994.

[8] J. Pei, J. Cai, D. Zou et al., "Design and performance validation of high-performance cement paste as a grouting material for semi-flexible pavement," *Construction and Building Materials*, vol. 126, pp. 206–217, 2016.

[9] S. Hou, T. Xu, and K. Huang, "Investigation into engineering properties and strength mechanism of grouted macadam composite materials," *International Journal of Pavement Engineering*, vol. 17, no. 10, pp. 878–886, 2016.

[10] S. Koting, M. R. Karim, H. Mahmud et al., "Effects of using silica fume and polycarboxylate-type superplasticizer on physical properties of cementitious grout mixtures for semiflexible pavement surfacing," *The Scientific World Journal*, vol. 2014, Article ID 596364, 7 pages, 2014.

[11] H. Yang, S. Zhang, L. Wang et al., "High-ferrite Portland cement with slag: hydration, microstructure, and resistance to sulfate attack at elevated temperature," *Cement and Concrete Composites*, vol. 130, pp. 104560–104576, 2022.

[12] Y. Peng, S. Tang, J. Huang, C. Tang, L. Wang, and Y. Liu, "Fractal analysis on pore structure and modeling of hydration of magnesium phosphate cement paste," *Fractal and Fractional*, vol. 6, pp. 337–355, 2022.

[13] L. Wang, Z. Yu, B. Liu, F. Zhao, S. Tang, and M. Jin, "Effects of fly ash dosage on shrinkage, crack resistance and fractal characteristics of face slab concrete," *Fractal and Fractional*, vol. 6, pp. 335–354, 2022.

[14] M. Guo, M. Liang, A. Sreeram, A. Bhasin, and D. Luo, "Characterisation of rejuvenation of various modified asphalt binders based on simplified chromatographic techniques," *International Journal of Pavement Engineering*, pp. 1–11, 2021.

[15] M. Guo, X. Liu, Y. Jiao, Y. Tan, and D. Luo, "Rheological characterization of reversibility between aging and rejuvenation of common modified asphalt binders," *Construction and Building Materials*, vol. 301, Article ID 124077, 2021.

[16] M. Guo, M. Liang, Y. Jiao, W. Zhao, Y. Duan, and H. Liu, "A review of phase change materials in asphalt binder and asphalt mixture," *Construction and Building Materials*, vol. 258, Article ID 119565, 2020.

[17] M. Gong, Z. Xiong, H. Chen et al., "Evaluation of the cracking resistance of semi-flexible pavement mixture by laboratory research and field validation," *Construction and Building Materials*, vol. 168, pp. 893–905, 2019.

[18] Q. J. Ding, Z. Sun, F. Shen, and S. L. Huang, "The performance analysis of semi-flexible Pavement by the volume parameter of matrix asphalt mixture," *Advanced Materials Research*, vol. 168-170, pp. 351–356, 2010.

[19] Q. Ding, M. Zhao, F. Shen, and X. Zhang, "Mechanical behavior and failure mechanism of recycled semi-flexible pavement material," *Material. J. Wuhan. Univ. Technol. (Materials Science Edition)*, vol. 30, no. 5, pp. 981–988, 2015.

[20] J. Cai, J. Pei, Q. Luo, J. Zhang, R. Li, and X. Chen, "Comprehensive service properties evaluation of composite grouting materials with high-performance cement paste for

semi-flexible pavement," *Construction and Building Materials*, vol. 153, pp. 544–556, 2017.

[21] X. Cai, H. Zhang, J. Zhang, X. Chen, J. Yang, and J. Hong, "Investigation on reinforcing mechanisms of semi-flexible pavement material through micromechanical model," *Construction and Building Materials*, vol. 198, pp. 732–741, 2019.

[22] X. Cai, L. Fu, J. Zhang, X. Chen, and J. Yang, "Damage analysis of semi-flexible pavement material under axial compression test based on acoustic emission technique," *Construction and Building Materials*, vol. 239, Article ID 117773, 2020.

[23] M. Gong, Z. Xiong, C. Deng, J. Yang, and J. Hong, "Influences of an artificial three-dimensional cementitious network on the fracture property of cement casting asphalt mixture," *Construction and Building Materials*, vol. 238, Article ID 117656, 2020.

[24] JTG E20 2011, *Standard Test Methods of Bitumen and Bituminous Mixtures for Highway Engineering*, Ministry of Transport of the People's Republic of China, China, 2011.

[25] AASHTO TP 124, "Standard method of test for determining the fracture potential of asphalt mixtures using semicircular Bend Geometry (SCB) at intermediate temperature," *American Association of State Highway and Transportation Officials*, vol. 124, no. 16, 2016.

[26] L. Mo, M. Huurman, S. Wu, and A. A. A. Molenaar, "Bitumen–stone adhesive zone damage model for the meso-mechanical mixture design of ravelling resistant porous asphalt concrete," *International Journal of Fatigue*, vol. 33, no. 11, pp. 1490–1503, 2011.

[27] L. Mo, M. Huurman, M. Woldekidan, S. Wu, and A. A. A. Molenaar, "Investigation into material optimization and development for improved ravelling resistant porous asphalt concrete," *Materials & Design*, vol. 31, no. 7, pp. 3194–3206, 2010.